

## Short-Time Inertial Response of Viscoelastic Fluids: Observation of Vortex Propagation

M. Atakhorrami,<sup>1,\*</sup> G. H. Koenderink,<sup>1,†</sup> C. F. Schmidt,<sup>1</sup> and F. C. MacKintosh<sup>1,2</sup>

<sup>1</sup>*Division of Physics and Astronomy, Vrije Universiteit, 1081HV Amsterdam, The Netherlands*

<sup>2</sup>*Isaac Newton Institute for Mathematical Sciences, University of Cambridge, Cambridge, CB3 0EH, United Kingdom*

(Received 14 April 2005; published 8 November 2005)

We probe the response of viscous and viscoelastic fluids on micrometer and microsecond length and time scales using two optically trapped beads. In this way we resolve the flow field, which exhibits clear effects of fluid inertia. Specifically, we resolve the short-time vortex flow and the corresponding evolution of this vortex, which propagates diffusively for simple liquids. For viscoelastic fluids, this propagation is shown to be faster than diffusive and the displacement correlations reflect the frequency-dependent shear modulus of the medium.

DOI: 10.1103/PhysRevLett.95.208302

PACS numbers: 83.60.Bc, 66.20.+d, 82.70.-y, 83.50.-v

A fundamental problem in hydrodynamics is the response of a liquid to the motion of a small embedded particle. At sufficiently long times, the well-known Stokes velocity field, which decreases as  $1/r$  away from the particle, will describe this fluid response. For an initial disturbance due to a local force in the liquid, however, only a small region of the liquid can be set in motion because of the inertia of the liquid. If the liquid is incompressible, backflow occurs that is characterized by a vortex ring surrounding the point disturbance. Since vorticity diffuses within the (linearized) Navier-Stokes equation, propagation of stress in the fluid drives the expansion of this vortex ring as a function of time  $t$  as  $\sqrt{t}$ . The  $1/r$  Stokes flow is established only in the wake of this vortex. While this basic picture has been known theoretically for simple liquids since Oseen [1], and has been observed in simulations since the 1960s [2], this vortex flow pattern has not been observed directly in experiment. Here, we use the correlations in thermal fluctuations of small probe particles to resolve this vortex flow field on the micrometer scale along with its diffusive propagation. We find good agreement between measured flow patterns and theoretical calculations for simple viscous fluids [1,3]. Furthermore, we demonstrate similar vortexlike flow in viscoelastic media, consistent with theoretical predictions in the accompanying Letter [4]. In the viscoelastic case, interestingly, vorticity spreads superdiffusively.

We obtain the spatial structure of the vortices by measuring the cross-correlated displacements of pairs of thermally excited colloidal particles in a fluid at frequencies up to 100 kHz. This technique is related to recent high resolution one- and two-particle microrheology experiments [5–8] used to probe the shear moduli of complex fluids. A schematic illustration of the experiment is shown in the inset of Fig. 1. By measuring the displacement cross correlations we obtain the mutual response functions of two spherical particles, labeled 1 and 2, where the coordinate axes are conveniently chosen to be parallel ( $x$ ) to the line connecting the particle centers and perpendicular ( $y$ ) to it. The mutual response function measures the displacement response of particle 2 to a force acting on particle 1 and

vice versa in the linear response regime. For separation distances  $r$  much larger than the particle radius  $R$ , the response function depends on  $r$  but not on particle size or shape [8,9].

The displacement  $u_x^{(1)}$  of particle 1 in the  $x$  direction is related to the force  $F_x^{(2)}$  acting on particle 2 according to  $u_x^{(1)}(\omega) = \alpha_{\parallel}(\omega)F_x^{(2)}$ , where  $\alpha_{\parallel}(\omega) = \alpha'_{\parallel}(\omega) + i\alpha''_{\parallel}(\omega)$  is the parallel complex response function with real and imaginary parts,  $\alpha'_{\parallel}(\omega)$  and  $\alpha''_{\parallel}(\omega)$ , and  $\omega$  is the radial frequency. Similarly, we define  $\alpha_{\perp}(\omega) = \alpha'_{\perp}(\omega) + i\alpha''_{\perp}(\omega)$ , with  $u_y^{(1)}(\omega) = \alpha_{\perp}(\omega)F_y^{(2)}$  for the perpendicular response function. The single-particle response functions for each  $x, y$  direction are defined as  $u_{x,y}^{(1)}(\omega) = \alpha_{\text{Auto}}(\omega)F_{x,y}^{(1)}$ . For homogeneous, isotropic media, these

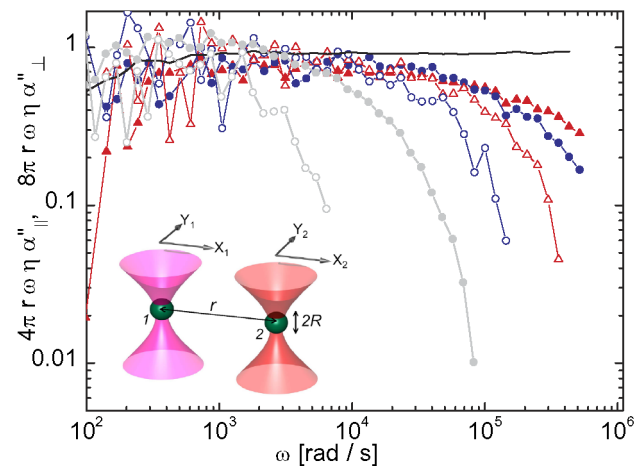


FIG. 1 (color online). Normalized responses of two particles,  $\parallel$  (filled) and  $\perp$  (open) in water/glycerol [ $r = 8.3 \mu\text{m}$  (blue, online);  $r = 5.7 \mu\text{m}$  (red, online)] compared to water ( $r = 8.3 \mu\text{m}$ ) in gray and to the normalized single-particle response function (horizontal line). For the same viscosity the decay shifts to lower frequency for larger  $r$  (blue, online). Inset: sketch of the experiment: two particles with separation  $r$  in two laser traps ( $\lambda = 830 \text{ nm}$ ,  $1064 \text{ nm}$ ). Displacements in the plane normal to the laser [parallel ( $x$ ) and perpendicular ( $y$ )] to the line of centers are detected using laser interferometry.

$\alpha_{\parallel,\perp}(\omega)$  completely characterize the linear response at any point in the medium to a force at another point. Both velocity and displacement response can be obtained from  $\alpha_{\parallel,\perp}(\omega)$ .

In the case of thermal excitations of two colloidal particles,  $\alpha_{\parallel,\perp}(\omega)$  also determine the correlations of these thermal fluctuations, via the fluctuation-dissipation theorem of statistical mechanics [10]. Accordingly, the imaginary parts  $\alpha''_{\parallel,\perp}(\omega)$  can be determined from the Fourier transform of the cross-correlated displacement fluctuations  $\langle u^{(1)}(t)u^{(2)}(0) \rangle$  of the two particles:

$$\alpha''_{\parallel}(\omega) = \frac{\omega \int \langle u_x^{(1)}(t)u_x^{(2)}(0) \rangle e^{i\omega t} dt}{2kT} \quad (1)$$

and  $\alpha''_{\perp}(\omega) = \frac{\omega \int \langle u_y^{(1)}(t)u_y^{(2)}(0) \rangle e^{i\omega t} dt}{2kT},$

where  $k$  is the Boltzmann constant and  $T$  is the temperature (in our experiments  $T = 21.5^\circ\text{C}$ , stabilized). Implicit in  $\alpha''_{\parallel,\perp}(\omega)$  is also a dependence on the (scalar) separation  $r$  between the two particles.

Our experiments were done with a custom-built inverted microscope [6,11] that provides a pair of focused laser beams with wavelengths  $\lambda = 830$  nm (diode laser), and  $\lambda = 1064$  nm (NdVO<sub>4</sub>). A pair of silica particles of radius  $R = 0.580 \mu\text{m} \pm 5\%$  are weakly trapped (trap stiffness  $\leq 3 \times 10^{-6}$  N/m), in a glass sample chamber with  $140 \mu\text{m}$  inner height; the experiments were performed at least  $25 \mu\text{m}$  from both surfaces. Displacements of the particles ( $x, y$ ) were detected by quadrant photo diodes [12], with a spatial resolution of  $\sim 0.1$  nm at 100 kHz bandwidth. For the 1064 nm laser light we used a specialized silicon PN photodiode (YAGG444-4A, Perkin Elmer), to avoid low-pass filtering [13]. Output voltages were digitized with an A/D interface (200 kHz) and recorded in Labview (National Instruments). The output voltages were calibrated [14] as described in [15].

We consider first the spatial structure of vortices in simple viscous liquids. As samples we used two Newtonian fluids with different viscosities  $\eta$  and mass densities  $\rho$ , namely, water ( $\eta = 0.969$  mPa s,  $\rho = 1000$  kg m<sup>-3</sup>) and a (1:1 v/v) water/glycerol mixture ( $\eta = 6.9$  mPa s,  $\rho = 1150$  kg m<sup>-3</sup>) for probe distances  $r$  between 2.2 and  $12 \mu\text{m}$ . Figure 1 shows representative data for  $\alpha''_{\parallel,\perp}(r, \omega)$  from pairs of silica particles, parallel to the center line (filled symbols) and perpendicular to it (open symbols) in water/glycerol [ $r = 8.3 \mu\text{m}$  (blue, online);  $r = 5.7 \mu\text{m}$ , (red, online)] and in water (gray symbols), ( $r = 8.3 \mu\text{m}$ ). The solid black line is the measured displacement autocorrelation of one of the particles from the same data. The experimental  $\alpha''(\omega)$  are normalized by their low-frequency limit (i.e., the Oseen tensor and Stokes drag coefficient), not yet accounting for fluid inertia [1]:  $\alpha''_{\parallel}(\omega) = 2\alpha''_{\perp}(\omega) = (4\pi r \omega \eta)^{-1}$  and  $\alpha''_{\text{Auto}}(\omega) = (6\pi R \omega \eta)^{-1}$ . With this normalization the data are expected to superimpose as a horizontal line for low frequencies.

The response  $\alpha''_{\text{Auto}}(\omega)$  does not deviate significantly from the Stokes limit over the full experimental frequency range. For  $\alpha''_{\parallel,\perp}(\omega)$ , however, a systematic decrease is seen at high frequencies, which reflects the failure of instantaneous, long-range stress propagation. For a given probe distance  $r$ ,  $\alpha''_{\perp}(\omega)$  turns down at lower frequencies than  $\alpha''_{\parallel}(\omega)$ . In the perpendicular channel, displacements become eventually anticorrelated (negative values not plotted), as expected from the backflow of the vortex-displacement field. As  $r$  increases, such anticorrelations are visible at lower frequency (blue, online). For the same  $r$ , the anticorrelation occurs in water at a lower frequency than in the water/glycerol mixture. The one-particle  $\alpha''_{\text{Auto}}(\omega)$  does not exhibit inertial effects in either of the two fluids studied, since the viscous penetration depths remain of order of or larger than the bead size [10,13,16].

The velocity response function for the fluid surrounding a moving sphere within the unsteady Stokes approximation was calculated by Oseen [1]. To compare with our  $\alpha''_{\parallel,\perp}(\omega)$ , we need the frequency dependence, which has the form [3,4]

$$\alpha''_{\parallel} = \frac{1}{4\pi r \omega \eta} \chi''_{\parallel} \left( r \sqrt{\frac{\rho \omega}{2\eta}} \right) \quad (2a)$$

and  $\alpha''_{\perp} = \frac{1}{8\pi r \omega \eta} \chi''_{\perp} \left( r \sqrt{\frac{\rho \omega}{2\eta}} \right),$

where

$$\chi''_{\parallel}(x) = \frac{e^{-x}}{x^2} [(1+x)\sin(x) - x\cos(x)] \quad (2b)$$

and  $\chi''_{\perp}(x) = \frac{e^{-x}}{x^2} [(x+2x^2)\cos(x) - (1+x)\sin(x)].$

Normalized  $\alpha''_{\parallel,\perp}(\omega)$  (e.g.,  $4\pi r \omega \eta \alpha''_{\parallel}$ ) for different viscous

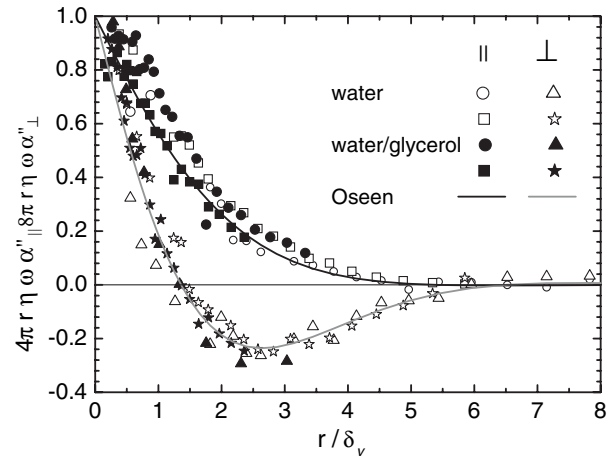


FIG. 2. Normalized responses, collapsed by plotting vs scaled separation distance  $r/\delta_v$  for  $r = 11.7 \mu\text{m}$  (circles, triangles),  $8 \mu\text{m}$  (square, stars), in water (open symbols,  $\eta = 0.969$  mPa s) and water/glycerol (filled symbols,  $\eta = 6.9$  mPa s). Normalized data fall onto the two master curves of Eq. (2) (dark and gray lines). Data shown for  $\omega > 200$  rad/s, for  $\omega < 2k$  rad/s one in every 5 data points.

liquids should thus collapse onto these master curves  $\chi''_{\parallel,\perp}$  when plotted versus distance normalized by the frequency dependent viscous penetration depth  $\delta_\nu = \sqrt{\eta/\omega\rho}$ .

Figure 2 demonstrates the expected collapse of our data for water and the water/glycerol mixture onto  $\chi''_{\parallel,\perp}$ , with no adjustable parameters. Figure 2 clearly shows the anticorrelation in the perpendicular channel at high frequencies, which is a direct consequence of the vortex flow. Scaling with  $\omega^{1/2}$  implicit in the data collapse demonstrates the diffusive propagation of this vortex. Prior experiments have reported diffusive propagation in longitudinal correlations between two particles in a Newtonian liquid [17], although transverse correlations (where backflow is apparent) were not observed. Here the  $\chi''_{\parallel,\perp}$  are defined such that  $\chi''_{\parallel,\perp}(\omega) \rightarrow 1$  as  $\omega \rightarrow 0$ . Thus the data collapse at low  $\omega$  is

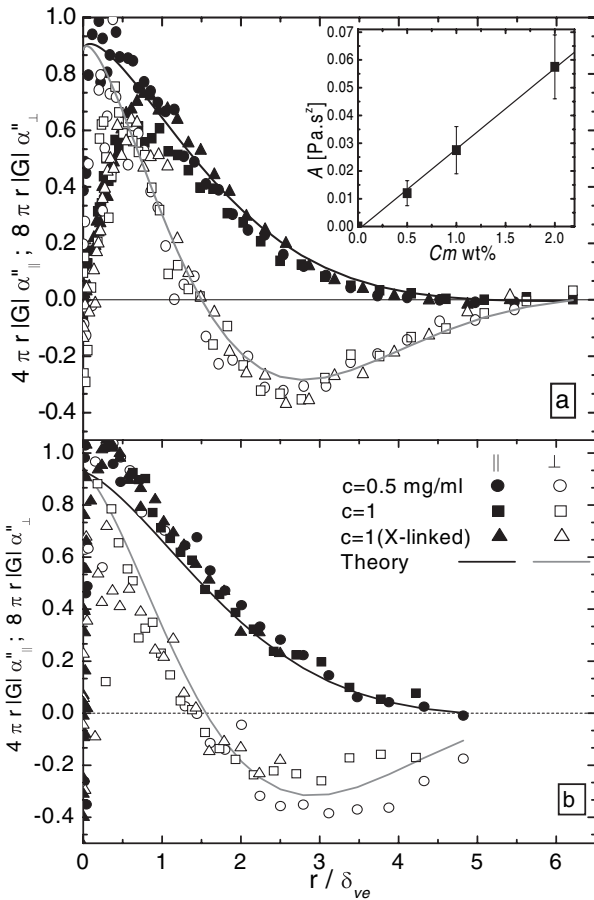


FIG. 3. Normalized responses  $4\pi r|G|\alpha''_{\parallel}$  (filled) and  $8\pi r|G|\alpha''_{\perp}$  (open) vs scaled distances  $r/\delta_{ve}$  for solutions of wormlike micelles, (a) [ $C_m = 0.5$  wt %,  $r = 8.3$   $\mu\text{m}$  (circles); 1 wt %,  $r = 10$   $\mu\text{m}$  (squares) and 2 wt %,  $r = 10$   $\mu\text{m}$  (triangles)]. (b) Entangled actin solutions with [ $C = 0.5$  mg/ml,  $r = 13.6$   $\mu\text{m}$  (circles); 1 mg/ml,  $r = 16.2$   $\mu\text{m}$  (squares)] and for weakly cross-linked actin network [ $C = 1$  mg/ml,  $r = 10.2$   $\mu\text{m}$  (triangles)]. Solid lines: predictions for a viscoelastic fluid with  $z = 0.68$  in micelles, and  $z = 0.75$  in actin. Inset of (a): the fit parameter  $A$  increases linearly with micelle concentration.

consistent with the static Oseen tensor. The vortex propagation is faster in the glycerol/water mixture than in water, since  $\eta/\rho$  is larger by a factor of 6.

In viscoelastic media [see accompanying Letter [4]], anticorrelations and oscillations are expected to be more pronounced. The vortex or stress propagation is also expected to be qualitatively different: it is no longer diffusive. In addition, polymer solutions are expected to have a larger penetration depth at a given frequency than a simple viscous fluid, given the higher modulus. We present experimental results from solutions of flexible, wormlike micelles, and solutions of entangled or sparsely cross-linked semiflexible actin filaments, both of which confirm the expectations.

We use wormlike micelles made from cetylpyridinium chloride (CPyCl) in brine (0.5 M NaCl) with sodium salicylate (NaSal) as counterions, molar ratio Sal/CPy = 0.5 (diameter 3 nm, persistence length 10 nm, length several  $\mu\text{m}$ ) [18]. We have measured  $\alpha''_{\parallel}$  and  $\alpha''_{\perp}$  for three different micelle concentrations ( $C_m$ ), and varying distances between the particles. Figure 3(a) shows the results for a particular distance in each concentration ( $C_m = 0.5$  wt %,  $r = 8$   $\mu\text{m}$ ; 1 wt %,  $r = 10$   $\mu\text{m}$ ; 2 wt %,  $r = 10$   $\mu\text{m}$ ).

We assume power-law behavior [4] for our viscoelastic solutions at high frequency, explicitly including the solvent:  $G = A(-i\omega)^z - i\omega\eta$ . Analogous to the viscous case presented in Fig. 2, the normalized compliances,  $4\pi r|G|\alpha''_{\parallel}$  and  $8\pi r|G|\alpha''_{\perp}$ , are plotted against particle separation scaled by the viscoelastic penetration depth,  $\delta_{ve} = \sqrt{|G|/\omega^2\rho}$ . In order to collapse data for different distances  $r$  and micelle concentrations we need to determine two adjustable (highly correlated) parameters, the exponent  $z$  and the (concentration-dependent) prefactor  $A$ . The exponent  $z$  for a semidilute solution of flexible polymers is expected to lie between 1/2 and 2/3 depending on hydrodynamic effects [19]. We found the best collapse of all data sets with each other and with the model curves for all five probed distances  $r$  (3–10  $\mu\text{m}$ ) and three concentrations, using a single  $z = 0.68 \pm 0.05$  and  $A = 0.012 \pm 0.0045$ ,  $A = 0.028 \pm 0.0085$ , and  $A = 0.0575 \pm 0.012$  Pa·s<sup>z</sup> for 0.5, 1, and 2 wt % micelles, respectively, [Fig. 3(a)] Our results are consistent with an expected linear concentration dependence of  $A$  (see inset). Furthermore, measured shear moduli in the low-frequency limit are in agreement with both macro- and micro-rheological measurements for wormlike micelles using different experimental methods [20]. The observed exponent  $z$  is consistent with the Zimm exponent of 2/3 [19]. The appearance of an elasticlike plateau of the shear modulus at low frequencies accounts for the observed downturn of both  $\alpha''_{\parallel}$  and  $\alpha''_{\perp}$  at low frequencies [11], which becomes more apparent for the concentrated micelle solutions.

F-actin is the polymeric form (filament diameter 7 nm, average length and persistence length  $\sim 17$   $\mu\text{m}$ ) of the major cytoskeletal protein actin. Entangled networks of

F-actin have high-frequency viscoelastic behavior qualitatively different from that of flexible polymer systems [21]. We looked at both entangled and weakly cross-linked networks of actin [22]. Figure 3(b) shows good data collapse after normalizing both  $\alpha''_{\parallel}$  and  $\alpha''_{\perp}$  for entangled actin at two concentrations (0.5 and 1 mg/ml) and for a weakly cross-linked actin gel (1 mg/ml). The best collapse of the data was found for parameters  $z = 0.8 \pm 0.1$  and  $A = 0.085 \pm 0.05, 0.18 \pm 0.13, 0.21 \pm 0.13 \text{ Pa s}^z$ , respectively. The actin solutions have a larger shear modulus than the micelle solutions, so the vortex-caused anticorrelation occurs at higher frequencies or larger separations. This is most evident in the case of the cross-linked actin solutions, with the highest shear modulus of all samples. Here, we see anticorrelation (backflow) set in only at  $\sim 40$  kHz, which leads to a larger inaccuracy in the determination of  $A$  and  $z$ . The viscoelastic exponent  $z$  found for actin solutions is consistent with  $z = 0.75$  [5,6,24] and because of the large error bars (particularly for  $A$ ) we chose  $z = 0.75$  to plot the data. The amplitude  $A$  is approximately a factor of 2 smaller than predicted [24].

We have shown how inertial flow in fluids can be directly resolved on micrometer and microsecond time scales using a new high-bandwidth laser interferometry technique. Inertia causes a vortexlike flow surrounding a localized disturbance at short times which leads to enhanced correlations in the thermal velocity fluctuations in liquids. A well-studied consequence of these correlations is the slow, algebraic decay of velocity correlations, known as the *long-time tail* [2], as can be seen in the crossover from ballistic to Brownian motion of colloidal particles [25]. This vortex flow leads to a diffusive propagation of stress in liquids, which is evident in our results. In viscoelastic media, however, the propagation of stress becomes superdiffusive as shown here. The implications of this for colloidal motion (e.g., long-time tail) in viscoelastic fluids have yet to be explored.

We thank T. Liverpool (theory), D. Mizuno (discussions), K. C. Vermeulen (actin purification), C. van Kats ( $\text{SiO}_2$  particles), and F. Gittes, J. Kwiecinska, and J. van Mameren (software). This work was supported by the Foundation for Fundamental Research on Matter (FOM).

\*Email address: maryam@nat.vu.nl

†Present address: Division of Engineering and Applied Sciences, Harvard University, Cambridge, MA 02138, USA.

- [1] C. W. Oseen, *Neuere Methoden und Ergebnisse in der Hydrodynamik* (Akademische Verlagsgesellschaft, Leipzig, 1927).
- [2] B. J. Alder and T. E. Wainwright, Phys. Rev. Lett. **18**, 988 (1967); Phys. Rev. A **1**, 18 (1970).
- [3] P. Mazur and D. Bedeaux, Physica (Amsterdam) **76**, 235 (1974).
- [4] T. B. Liverpool and F. C. MacKintosh, this issue, Phys. Rev. Lett. **95**, 208303 (2005).
- [5] F. Gittes, B. Schnurr, P. D. Olmsted, F. C. MacKintosh, and C. F. Schmidt, Phys. Rev. Lett. **79**, 3286 (1997).
- [6] B. Schnurr, F. Gittes, F. C. MacKintosh, and C. F. Schmidt, Macromolecules **30**, 7781 (1997).
- [7] J. C. Meiners and S. R. Quake, Phys. Rev. Lett. **82**, 2211 (1999).
- [8] J. C. Crocker, M. T. Valentine, E. R. Weeks, T. Gisler, P. D. Kaplan, A. G. Yodh, and D. A. Weitz, Phys. Rev. Lett. **85**, 888 (2000).
- [9] A. J. Levine and T. C. Lubensky, Phys. Rev. Lett. **85**, 1774 (2000).
- [10] L. D. Landau and E. M. Lifshitz, *Fluid Mechanics* (Butterworth-Heinemann, Oxford, 2000).
- [11] M. Atakhorrami *et al.* (to be published).
- [12] F. Gittes and C. F. Schmidt, Opt. Lett. **23**, 7 (1998).
- [13] E. J. G. Peterman, M. A. van Dijk, L. C. Kapitein, and C. F. Schmidt, Rev. Sci. Instrum. **74**, 3246 (2003).
- [14] In viscous liquids the detection was calibrated using the same beads as used for the correlation measurements; in the viscoelastic systems calibration was done separately in water.
- [15] F. Gittes and C. F. Schmidt, *Meth. Cell. Biol.* (Academic, New York, 1998), Vol. 55, p. 129.
- [16] K. Berg-Sørensen and H. Flyvbjerg, Rev. Sci. Instrum. **75**, 594 (2004).
- [17] S. Henderson, S. Mitchell, and P. Bartlett, Phys. Rev. Lett. **88**, 088302 (2002).
- [18] J. A. J. F. Berret and G. Porte, Langmuir **9**, 2851 (1993).
- [19] M. Doi and S. F. Edwards, *The Theory of Polymer Dynamics* (Oxford University Press, New York, 1986).
- [20] M. Buchanan, M. Atakhorrami, J. F. Paliarne, F. C. MacKintosh, and C. F. Schmidt, Phys. Rev. E **72**, 011504 (2005).
- [21] F. C. MacKintosh and P. A. Janmey, Curr. Opin. Solid State Mater. Sci. **2**, 350 (1997).
- [22] Monomeric actin (G-actin) was isolated from rabbit skeletal muscle [23], mixed with silica beads, and polymerized for 1 h at a concentration of 1 mg/ml by addition of concentrated buffer (final concentration 2 mM HEPES, 2 mM  $\text{MgCl}_2$ , 50 mM KCl, 1 mM  $\text{Na}_2\text{ATPa}$ , and 1 mM EGTA, pH 7). Cross-linked networks with a low-frequency plateau elastic modulus of 0.8 Pa were obtained by copolymerizing a small fraction of biotinylated G-actin with unlabeled G-actin, and adding neutravidin (Pierce Biotechnology) at molar ratios actin/biotinylated actin = 50 and actin/neutravidin = 200.
- [23] J. D. Pardee and J. A. Spudich, Methods Enzymol. **85**, 164 (1982).
- [24] D. C. Morse, Phys. Rev. E **58**, R1237 (1998); F. Gittes and F. C. MacKintosh, Phys. Rev. E **58**, R1241 (1998).
- [25] G. L. Paul and P. N. Pusey, J. Phys. A **14**, 3301 (1981); D. A. Weitz, D. J. Pine, P. N. Pusey, and R. J. A. Tough, Phys. Rev. Lett. **63**, 1747 (1989).